Resonances between fluxons and plasma waves in underdamped Josephson transmission lines of stripline geometry

J. Pfeiffer, A. A. Abdumalikov, Jr., M. Schuster, and A. V. Ustinov*
Physikalisches Institut III, Universität Erlangen-Nürnberg, D-91058 Erlangen, Germany
(Received 1 May 2007; revised manuscript received 16 October 2007; published 14 January 2008)

We present experiments and theoretical studies on the propagation of Josephson fluxons and electromagnetic waves in parallel arrays of Josephson junctions in the limit of small discreteness. Locking between the fluxon rotation frequency and the frequency of the radiated electromagnetic waves leads to a series of resonances, which we observe on the dc-current-voltage characteristics of the arrays. The arrays consist of small Josephson junctions embedded in an annular superconducting stripline. The experimental data are analyzed using the discrete sine-Gordon model and an extension by including a capacitive interaction between neighboring Josephson junctions. We compare experimental data with both analysis and numerical simulations and find an excellent quantitative agreement.

DOI: 10.1103/PhysRevB.77.024511 PACS number(s): 74.50.+r, 05.45.Yv, 74.81.Fa, 85.25.Cp

I. INTRODUCTION

During the past decades, much attention has been paid to the discrete version of the perturbed sine-Gordon (SG) equation. It describes the dynamics of topological excitations in various spatially modulated systems, e.g., dislocations in crystals, magnetic and ferroelectric domain walls in various condensed matter systems, and vortices in arrays of superconducting Josephson junctions.[1] The behavior of these systems is often strongly overdamped and thus the inertia of topological kinks played no role. In the opposite limit, where the damping is small, ballistically moving kinks interact with a discrete lattice and generate linear excitations.[2,3] A unique system, in which this interaction can be studied with great flexibility and precision, is a parallel array of small Josephson junctions, often also called Josephson transmission line. Presently, only few experiments have been carried out with underdamped arrays of such junctions.[4–8]

There are two important types of excitations existing in parallel arrays of Josephson junctions—nonlinear excitations in the form of Josephson phase kinks along the array and small-amplitude phase oscillations, which are linear. A Josephson phase kink is often called a *fluxon*, as it is a vortex of supercurrent generating a magnetic flux equal to the magnetic flux quantum Φ_0 (see Fig. 1). Peyrard and Kruskal[3] pointed out that even for large discreteness a topological kink in the SG lattice exhibits solitonic features. The essential feature introduced by the discreteness of the lattice, is the radiation of linear waves by a moving kink:[2] As the kink moves through the lattice, it excites small-amplitude linear waves in its wake. Due to their plasma-type dispersion relation, these linear oscillations are often referred to as Josephson plasma waves. As the radiated waves dissipate energy, the movement of the kink can only be maintained by applying a driving force. In the equilibrium case, the velocity of the kink is constant due to energy balance between applied and dissipated energy. The driving force versus velocity relation of a kink can be measured in experiment, revealing the dynamic properties of the system.

In studying the propagation of linear and nonlinear waves in arrays of Josephson junctions, it is desirable to avoid influences of the array boundaries. Therefore, in this paper, we focused on experiments with arrays of annular geometry, thus having periodic boundary conditions. Our experimental realization of an annular array of Josephson junctions is schematically shown in Fig. 1. In such a system, a fluxon rotating around the array at certain frequencies can resonate with the frequency of the plasma waves in its own tail.[10] Simulations showed that the interaction between a moving fluxon and the radiated plasma waves is manifested by resonant steps on the current-voltage characteristics at voltages corresponding to the resonating velocities.[10] Up to now, these plasma wave resonances were experimentally observed[5] in annular junction arrays with *planar* cells. The voltage positions and thus the frequencies of the steps observed in the first experiments[5–8] were in good agreement with the expected locking conditions[10] mentioned below in this paper [see Eq. (1)]. However, the overall shape of the resonant steps was not well reproduced in numerical simulations.

In this paper, we present a detailed experimental and numerical study of fluxon dynamics in annular parallel arrays of underdamped Josephson junctions. We go beyond previous experimental works that were based on the planar array geometry[5–8] and study here arrays of a different configuration, which we refer to as *stripline* geometry. We observe plasma wave resonances for a single fluxon revolving in the array. The experimental results are analyzed by using two different approaches. First, we examine the experimental data using the conventional discrete SG equation. Further-

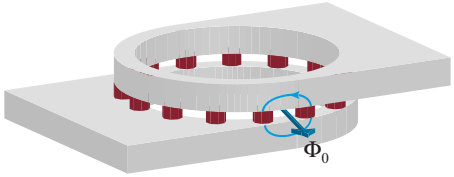

FIG. 1. (Color online) Schematic drawing of a one-dimensional parallel array of Josephson junctions having the stripline geometry. The junctions are colored dark red (dark gray). A fluxon is indicated in blue (arrow).

more, by following the idea of Ref. 12, we develop a more detailed model, which also includes the capacitive interactions between individual Josephson junctions. The capabilities of both models are compared to the experiment. To gain a deeper insight in the dynamics of the system, we carried out a comparison between experimental data and numerical simulations. We found a striking quantitative agreement. The shape of the resonant steps measured in experiment resembled exactly the simulated curves. Such a remarkable agreement has not been seen in any of the experiments reported to date.

II. EXPERIMENTAL RESULTS

The one-dimensional parallel arrays of Josephson junctions are fabricated in a Nb-Al/AlO_x-Nb trilayer technology.[13] The junctions are equidistantly embedded in an annular stripline. A schematic drawing of one sample is shown in Fig. 1. The array parameters are defined by its geometrical dimensions, the thickness of the silicon dioxide layer between the junctions and their critical currents. In this paper, we present experimental data obtained for four arrays. These arrays have the same ring diameter of 355 μm, but contain a different number of junctions N, namely, $N=12$, 16, 20, and 25. The area of all Josephson junctions is 5×5 μm^2, and the critical current per junction is $I_c=50$ μA. Using the measured array parameters, we are able to calculate directly the SG discreteness parameter a for the different samples [see Eq. (3)]. Measurements were performed in a magnetically shielded environment using a cryostat with stabilized variable temperature.

We study the fluxon motion in the array by measuring its dc-current-voltage characteristics (*IV*C). The *IV*C trace directly reveals the relationship between the average fluxon velocity v, which is proportional to the measured dc voltage V, and the driving force γ, which is proportional to the bias current I. To trap one fluxon or several fluxons in the array, we cool the sample through the superconducting transition temperature of Nb in the presence of a small bias current. The flux is trapped spontaneously. Due to the flux quantization in superconducting rings, the initial number of fluxons trapped in the array is conserved as long as the critical temperature is not crossed during experiment. Below, we present measured *IV*Cs with a single fluxon trapped in the array.

The low voltage part of a *IV*C of a single-fluxon state for the array with $N=25$ junctions is shown in Fig. 2. In order to record this curve, we increase the bias current starting from zero until the fluxon overcomes the Peierls-Nabarro barrier[14] at $I=I_{PN}$. The Peierls-Nabarro barrier characterizes the pinning of a kink induced by the SG lattice and strongly depends on the discreteness parameter a. In the limit of small discreteness, the Peierls-Nabarro barrier and, thus, the depinning current should be small.[15] The relatively high depinning current that is seen in Fig. 2 can be explained by parasitic pinning in the array due to additional current injectors attached to the array. In the presented experiments, we did not use these injectors to trap flux. Once overcoming the Peierls-Nabarro barrier, the fluxon starts to travel around the array and produces a nonzero dc voltage, the single-fluxon step. At

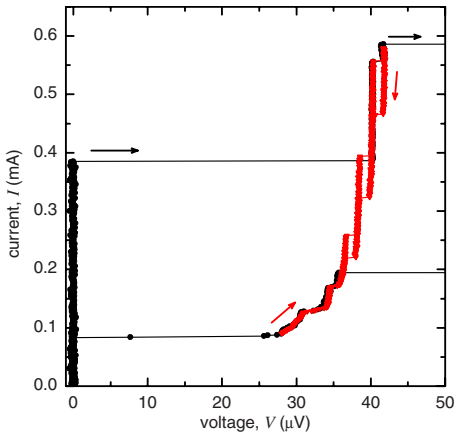

FIG. 2. (Color online) Experimental data of *IV*C measurements of the single-fluxon step in an array with $N=25$ junctions. The arrows denote the sweeping direction of the bias current. The return path is traced out separately and is shown in red (dark gray). The experimental data are obtained at a temperature of $T=6.17$ K.

the very top of the single-fluxon *IV*C step, the array switches to the high voltage state. Then, the bias current is decreased down to zero (see black dots in Fig. 2). During the second measurement, the bias current I is increased slightly above the depinning current I_{PN} and subsequently decreased. In this range, by sweeping the bias current up and down, we reveal a fine structure on the single-fluxon step. These resonant steps have nearly constant voltages and show a hysteretic behavior.

The single-fluxon characteristics of all four arrays are compared in Fig. 3. The measurement procedure in all cases is the same, as described in relation to Fig. 2. Among all four samples, common features are evident. The voltage position of the single-fluxon *IV*C decreases with an increasing junc-

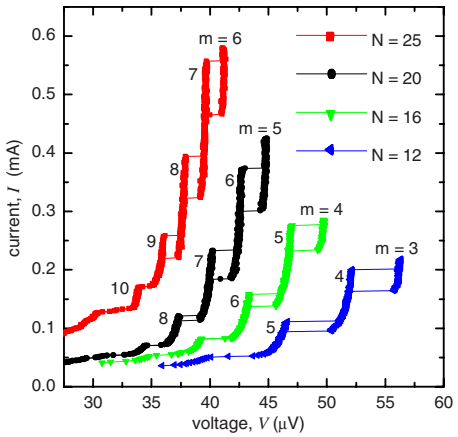

FIG. 3. (Color online) A single-fluxon step was measured in four arrays of Josephson junctions. All curves show plasma wave resonances. The respective resonance index m is indicated at the left of every step. The temperatures of the measurements are estimated from the gap voltage according to its theoretically expected dependence (Ref. 16). The temperatures are given as $T=6.77$ K for $N=12$, $T=6.53$ K for $N=16$, $T=6.56$ K for $N=20$, and $T=6.17$ K for $N=25$. All arrays have the same diameter of $\oslash 355$ μm.

tion number N. Furthermore, the voltage spacing between smaller steps on each curve also decreases with an increasing number of junctions in the array. The fine structures shown in Fig. 3 are only clearly resolved in a narrow temperature interval of $T=6-7$ K. This temperature interval depends on the respective sample and its parameters. In general, we found that the higher the number junctions (and thus smaller the array discreteness), the lower the temperature required to observe the fine structures. The specific temperatures for our data are indicated in the caption of Fig. 3. Increasing temperature reduces the hysteresis between fine structure resonances and smears them out. At the lowest temperatures of their observation range, the resonances on *IV*C become unstable, and the array switches from superconducting state to high voltages corresponding to the energy gap.

We have also measured states with a larger number of fluxons trapped in the array. Fine structures comparable to those seen in Fig. 3 were also observed for the second, third, and higher fluxon steps as well as zero field steps[19] (data not shown). In the limit of a small discreteness parameter $a \ll 1$, we found no qualitative difference between resonances on the first and higher fluxon steps. It should be stressed that in the case of a larger discreteness parameter $a \geqslant 1$, there are interesting bunching effects, which are observed if more than one fluxon is trapped in the array.[9]

III. THEORETICAL MODELS

The fine structures observed in our experiments very much resemble that of the original numerical simulations.[10] The nearly constant-voltage steps occur due to resonances between the traveling fluxon and the plasma oscillations in the fluxon tail. Under periodic boundary conditions, the resonances with number m occur when the passage of the fluxon through a given point of the array coincides with the mth maximum of the oscillations induced by the plasma wave trailing behind the fluxon. That would mean that the junction length should accommodate m wavelengths of the plasma wave. In order to quantitatively find the resonance condition for our rings, we have used two different approaches. The first approach is based on the perturbed discrete sine-Gordon equation described in Sec. III A. The second approach uses a generalized model, which was initially developed in Ref. 12. In both cases, the resonance condition can be written as

$$\omega_m = k_m v_m, \tag{1}$$

where ω_m is the angular frequency of the plasma waves, k_m is their wave number, v_m is the fluxon velocity at the resonance, and m is the resonance index. Condition (1) requires the phase velocity of the waves ω_m/k_m equaling the velocity of the kink v_m, which is the condition for the Cherenkov radiation. Hence, the resonances that we observed in our experiment are induced by the Cherenkov radiation of a kink moving through a discrete lattice.

A. Discrete sine-Gordon model

A one-dimensional array of Josephson junctions is usually described by the discrete SG equation

$$\frac{\varphi_{n+1} - 2\varphi_n + \varphi_{n-1}}{a^2} - \frac{d^2\varphi_n}{dt^2} = \sin\varphi_n + \alpha\frac{d\varphi_n}{dt} - \gamma. \tag{2}$$

Here, φ_n is the phase difference across the nth junction, $0 \leqslant n \leqslant N$. Equation (2) is written using the standard notation:[10] The time is normalized to the inverse of plasma frequency $\omega_p = \sqrt{2\pi I_c/\Phi_0 C}$, $\alpha = \sqrt{\Phi_0/2\pi I_c R^2 C}$ is the damping coefficient, and

$$a = \sqrt{\frac{2\pi L_{\text{self}} I_c}{\Phi_0}} \tag{3}$$

is the discreteness parameter. Here, C is the capacitance of a single junction, R is its differential resistance, and L_{self} is the geometrical inductance of a single cell. γ is the bias current per junction normalized to its critical current I_c. The coupling between neighboring junctions is characterized by the coupling constant $1/a^2$. The larger the lattice spacing and, thus, the discreteness parameter a, the smaller the coupling between the individual junctions. Here, we neglected surface losses as they are estimated in our case (temperatures above 4.2 K for niobium junctions) to be at least 1 order of magnitude smaller than the losses given by the α term.[11]

As pointed out in Ref. 17, Eq. (2) can be linearized around a solution $\varphi_n(t) = \varphi_n^*(t) + u_n(t)$, which represents the traveling kink and a small perturbation. For a linear mode of the form $u_n(t) = \exp[i(\omega t + kna)]$, it is straightforward to obtain the dispersion relation

$$\omega = \sqrt{\kappa + \frac{4}{a^2}\sin^2\left(\frac{ka}{2}\right)}. \tag{4}$$

Here, κ is the contraction factor in mean field treatment,[17] which is defined as

$$\kappa = \frac{1}{N}\sum_{n=1}^{N}\cos\varphi_n^*. \tag{5}$$

This factor takes into account phase shifts induced by the kink solution $\varphi_n^*(t)$ and the bias current γ on the oscillation-free state of the lattice. In the case of a small number of junctions N and/or small discreteness parameter a, the topological structure of the kink has the strongest effect on the contraction factor κ. Furthermore, the factor κ depends on the applied bias current γ. In this paper, we consider the single-kink states of relatively long arrays with rather large discreteness parameter a; thus, the contraction factor at zero bias is small. We take the contraction factor into account as $\kappa = \cos\arcsin\gamma = \sqrt{1-\gamma^2}$, resulting in a typical value of $\kappa \approx 0.5$ in the current range of the observed resonances (for details, see Refs. 18 and 19).

By using Eqs. (1) and (4), one obtains the following expression for the voltages of the resonances:[10]

$$V_m = \frac{1}{m}\frac{\Phi_0}{2\pi\sqrt{L_{\text{self}}C}}\sqrt{\kappa a^2 + 4\sin^2\left(\frac{m\pi}{N}\right)}. \tag{6}$$

Here, m is the number of plasma wave oscillations per circulation period of the fluxon.

B. Capacitive discrete sine-Gordon model (Fistul-Caputo-Ustinov model)

The discrete SG model [Eq. (2)] takes into consideration only inductive interactions between neighboring Josephson junctions. The junctions are assumed to be lumped elements. Capacitive interactions between neighboring junctions were taken into account by Fistul, Caputo, and Ustinov (FCU).[12] Their model is referred to in the following as the FCU model. The authors derived the dispersion relation for linear waves in the high voltage limit, i.e., neglecting the supercurrent through the junctions. In the framework of this model, the dispersion relation of linear waves contains many bands. In the following section, we generalize the above work by including supercurrents. We derive the dispersion relation for linear waves in the low voltage limit in order to calculate the resonant voltages on the first fluxon step.

A parallel array of stripline geometry shown in Fig. 1 can be viewed as a lattice of small inhomogeneities (Josephson junctions) embedded in a medium without Josephson coupling (passive superconducting stripline). The Josephson phase difference depends on the spatial coordinate x and the time t. Using the continuum version of the SG model for the Josephson junction region and the Laplace equation for the transmission line region, we obtain

$$\frac{\partial^2\varphi}{\partial x^2} - \frac{1}{b^2\omega_g^2}\frac{\partial^2\varphi}{\partial t^2} - \xi(x-x_n)\left[\frac{1}{b^2\omega_g^2}\left(\frac{b}{\eta l}-1\right)\frac{\partial^2\varphi}{\partial t^2} + \frac{a^2}{bl}\sin\varphi + \frac{L_{\text{self}}}{b\rho}\frac{\partial\varphi}{\partial t}\right] = -\xi(x-x_n)\frac{a^2\gamma}{bl}. \tag{7}$$

Here, b is the distance between two neighboring junctions, l is the size of one junction along the transmission line, ρ is the transmission line resistivity, and L_{self} is the inductance per cell. The Josephson junctions are described by the function $\xi(x-x_n)$, where $x_n=n(b+l)$ is the coordinate of the center of the nth junction. The characteristic angular frequency of electromagnetic field oscillations in the transmission line is $\omega_g=\sqrt{C_0 L_{\text{self}}}$, where C_0 is the capacitance of the transmission line between two neighboring junctions. The parameter $\eta=C_0/C$ characterizes the strength of the capacitive coupling between the junctions.

In order to obtain the dispersion relation for linear waves, we use an ansatz $\varphi(x,t)=\varphi_0+\varphi_1(x)e^{i\omega t}$, where φ_0 is an exact fluxon-free solution of Eq. (7) at a constant bias current γ. Using Bloch's theorem, the dispersion relation for linear waves is obtained in the transcendental equation form

$$\cos[\kappa(b+l)] = \cos(\theta a)\cos(\beta l) - \frac{\theta^2+\beta^2}{2\theta\beta}\sin(\theta a)\cos(\beta l), \tag{8}$$

with

$$\theta = \frac{\omega}{b\omega_g} \tag{9}$$

and

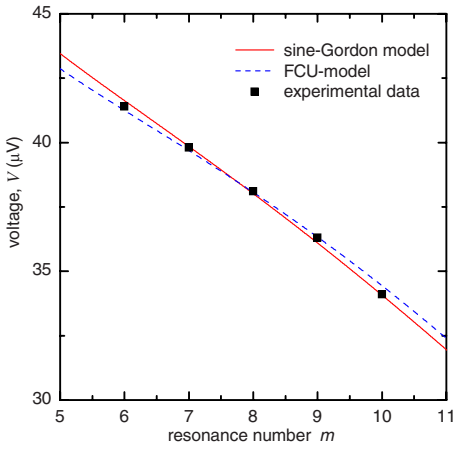

FIG. 4. (Color online) Comparison between the SG model, the FCU model, and the experimental data.

$$\beta = \sqrt{\frac{\omega^2}{b^2\omega_g^2}\frac{b}{\eta l} - \kappa\frac{a^2}{bl}}. \tag{10}$$

The voltage positions V_m of plasma wave resonances in this model are given by

$$V_m = \frac{\Phi_0\omega(k_m)}{2\pi m}. \tag{11}$$

Here, $\omega(k)$ is the dispersion relation obtained numerically from Eq. (8) and m is the number of oscillations between consecutive passages of the fluxon.

C. Comparison with experimental data

We have examined whether the experimental data shown in Fig. 2 can be reproduced within the framework of both models presented above. We used the voltages measured at the top of each resonant step taken from Fig. 2 as the experimental values V_m^{exp}. Equations (6) and (11) are fitted to the experimental data V_m^{exp} using a nonlinear least squares fit. In both fits, we used

$$L_{\text{self}} = \frac{\mu_0 b(2\lambda_L + t_0)}{W} = 2.3\times 10^{-12}\ \text{V s/A}. \tag{12}$$

Here, W is the transmission linewidth, b is the distance between neighboring Josephson junctions, λ_L is the London penetration depth, which is provided by the manufacturer as 87 ± 5 nm,[13] and t_0 is the thickness of the Josephson tunnel barrier. These values are defined by the fabrication process as $W=21$ μm, $b=40$ μm, and $t_0=0.9$ μm. The value of C_0 is calculated from geometrical considerations as $C_0=0.044$ pF. The capacitance of a single Josephson junction C is used as the fitting parameter for both the SG model and the FCU model, giving $C=1.4$ and 1.5 pF, respectively. In Fig. 4, both fits and the experimental data are shown. The standard deviations between experimental and fitted data are $\sigma=0.15$ μV (SG model) and $\sigma=0.18$ μV (FCU model).

Obviously, both models agree very well with the experimental data. The difference between the capacitances found by using the SG model and the FCU model is tiny. Thus, we

conclude that the capacitive interactions between the Josephson junctions in our stripline arrays are negligible and the conventional SG model is good enough to describe the experiment.

IV. NUMERICAL SIMULATIONS

We carried out numerical simulations for an array with $N=25$ and compared them with the experimental current-voltage characteristics shown in Fig. 2. The simulations are performed by integrating the perturbed discrete SG equation [Eq. (2)] using the fourth-order Runge-Kutta scheme[10] with periodic boundary conditions

$$\varphi_N = \varphi_0 + 2\pi M_{\mathrm{fl}},$$

where $M_{\mathrm{fl}}=1$ is the number of fluxons trapped in the array. The integration time chosen as 500 normalized time units eliminated the transients due to the change of γ at every bias point. The integration time step is set as 0.02 and the current increment is $\Delta\gamma=0.005$.

The discreteness parameter of the experimental data with $N=25$ is calculated according to Eq. (3), giving $a\simeq 0.5$. The value of the critical current I_c of a single Josephson junction is obtained directly from measurements. The damping parameter[20] α is chosen as $\alpha=0.1$. The *IV*C simulated with the above values resembles our typical experimental curves in terms of both step shape and their current range. The average calculated voltage v is normalized to $2\pi/\ell$, thus yielding the average fluxon velocity normalized to the one in a continuous Josephson junction of length ℓ. In order to reveal a hysteretic behavior of the steps on the current-voltage characteristics, the current is swept up and down, similar to the experiment.

In good agreement with the experiment, we obtained resonant substeps on the numerically simulated current-voltage characteristics. The insets in Fig. 5 show traces of the voltage versus time for three different steps of the *IV*C. Increasing the bias current along each step does not lead to any significant increase of the voltage because the energy fed by the bias current is consumed to amplify the amplitude of the plasma waves and not to accelerate the fluxon. The voltage versus time plot of the highest resonant step reveals clear oscillations between consecutive passages of the kink, yielding $m=6$ periods of plasma waves between every two kink maxima.

To directly compare the simulations to the experimental data, the simulated data are converted to physical units by using $I=\gamma N I_c$ and $V=(\Phi_0\omega_p v)/2\pi$. To obtain a better agreement between the simulated curve and the measured data, we finely adjusted the critical current I_c and the damping parameter. It has been known that varying the damping parameter α between 0.05 and 0.3 does not significantly change the voltage position of the resonance steps,[10] but influences the slope of the *IV*C and the shape of the hysteretic loops. The lower α is, the steeper is the overall slope of the current-voltage characteristics, and the larger is the hysteresis of the steps. Thus, by varying α, the agreement between the shape of the simulated and the experimental curve can be improved. A proportional scaling of the critical current I_c shifts the simulated curve along the vertical axis. We found the best fits with an absolute critical current adjustment by ±5% and α chosen as 0.08. We believe that this adjustment procedure is justifiable due to the uncertainty of the experimental values of I_c and α.

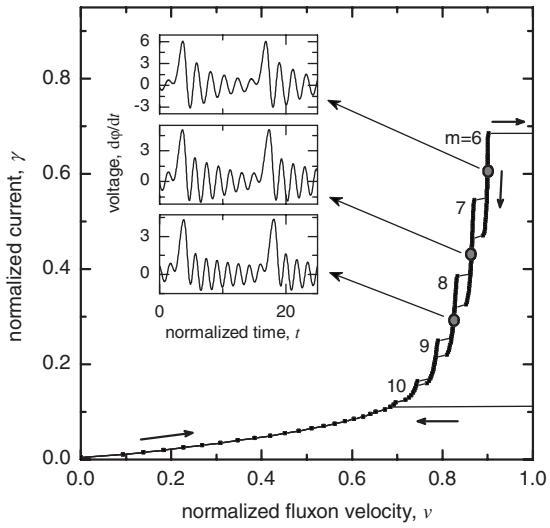

FIG. 5. A simulated *IV*C of a parallel array with $N=25$, $a=0.5$, and $\alpha=0.08$. The insets show the voltage versus time evolution for three resonance steps. The voltage evolution is measured at a single arbitrary chosen junction.

The simulated current-voltage characteristics are superimposed with the experimental data in Fig. 6. The agreement is excellent. The position of the resonant steps and their voltage spacing, as well as the overall shape of the *IV*C, are quantitatively reproduced. The *IV*Cs of the three other rings shown in Fig. 3 are simulated in the same way and show a comparably good agreement with experiment[19] (data not shown here).

We note that the resonances studied in this paper can be practically useful for the generation of high harmonics of the fluxon oscillation frequency. The frequency of the strongest harmonic can be tuned continuously by bias current in a

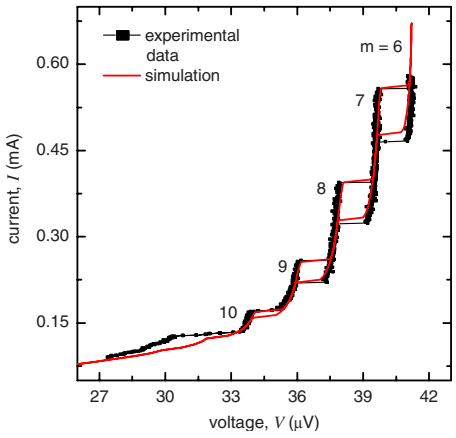

FIG. 6. (Color online) Comparison between experimental data (black) and simulated current-voltage characteristics (red/gray) with $N=25$, $a=0.5$, and $\alpha=0.08$.

small range and also steplike by changing the harmonic number.

In summary, we studied in detail fluxon dynamics in one-dimensional parallel Josephson arrays in the limit of low damping. We observed plasma wave resonances induced by phase locking between a moving fluxon and its radiation in the junction cavity. We have found an excellent agreement between simulations, theory, and experimental data.

*ustinov@physik.uni-erlangen.de

[1] J. M. Yeomans, Solid State Phys. **41**, 151 (1988).
[2] J. F. Curie, S. E. Trullinger, A. R. Bishop, and J. A. Krumhansl, Phys. Rev. B **15**, 5567 (1977).
[3] M. Peyrard and M. D. Kruskal, Physica D **14**, 88 (1984).
[4] M. Cirillo, B. H. Larsen, A. V. Ustinov, V. Merlo, V. A. Oboznov, and R. Leoni, Phys. Lett. A **183**, 383 (1993).
[5] H. S. J. van der Zant, T. P. Orlando, S. Watanabe, and S. H. Strogatz, Phys. Rev. Lett. **74**, 174 (1995).
[6] S. Watanabe, S. H. Strogatz, H. S. J. van der Zant, and T. P. Orlando, Phys. Rev. Lett. **74**, 379 (1995).
[7] S. Watanabe, H. S. J. van der Zant, S. H. Strogatz, and T. P. Orlando, Physica D **97**, 429 (1995).
[8] A. V. Ustinov, M. Cirillo, B. H. Larsen, V. A. Oboznov, P. Carelli, and G. Rotoli, Phys. Rev. B **51**, 3081 (1995).
[9] J. Pfeiffer, M. Schuster, A. A. Abdumalikov, and A. V. Ustinov, Phys. Rev. Lett. **96**, 034103 (2006).
[10] A. V. Ustinov, M. Cirillo, and B. A. Malomed, Phys. Rev. B **47**, 8357 (1993).
[11] A. Franz, M.S. thesis, Erlangen, 1999 (http://fluxon.physik.uni-erlangen.de).
[12] M. V. Fistul, P. Caputo, and A. V. Ustinov, Phys. Rev. B **60**, 13152 (1999).
[13] Jena Superconducting Electronics Foundry, IPHT, Jena, Germany.
[14] R. Peierls, Proc. Phys. Soc. London **52**, 34 (1940).
[15] A. Ambegaokar and A. Baratoff, Phys. Rev. Lett. **11**, 104(E) (1963).
[16] B. Muehlschlegel, Z. Phys. **155**, 313 (1959).
[17] Z. Zheng, B. Hu, and G. Hu, Phys. Rev. B **58**, 5453 (1998).
[18] M. Schuster, M.S. thesis, Erlangen, 2000 (http://fluxon.physik.uni-erlangen.de).
[19] J. Pfeiffer, M.S. thesis, Erlangen, 2005 (http://fluxon.physik.uni-erlangen.de).
[20] It is somewhat ambiguous to calculate α directly from experiment as it depends on the subgap differential resistance, which changes around the single-fluxon step. Usually, the values of α chosen close to 0.1 give the best agreement with experimental data.